Available online at www.sciencedirect.com
ScienceDirect
Journal of Sound and Vibration 311 (2008) 874–885
JOURNAL OF SOUND AND VIBRATION
www.elsevier.com/locate/jsvi

Reducing position error signal (PES) due to disk vibration using an air shroud

Zhimin He*, Chunling Du, Jianqiang Mou, Eng Hong Ong

*A*Star, Data Storage Institute, 5, Engineering Drive 1 (off Kent Ridge Crescent, NUS), Singapore 117608, Singapore*

Received 2 March 2007; received in revised form 4 July 2007; accepted 25 September 2007
Available online 7 November 2007

Abstract

The advances in magnetic recording technology demand higher magnetic head positioning accuracy and faster disk rotation speed. However, the higher rotational speed of disk generates the greater flow-induced vibration known as disk flutter, which causes the increase of the track misregistration (TMR). To overcome the issue, an air shroud is presented to reduce disk vibration and position error signal (PES) for magnetic recording. Computational fluid mechanics simulations are performed to study the flow pattern surrounding a disk with an air shroud for different openings. The air-bearing stiffness and damping effects of the disk spindle assembly with an air shroud are evaluated. Based on the computational fluid dynamics (CFD) simulation, the air shroud is prototyped and the disk vibrations with and without the air shroud at different disk rotation speeds are experimentally investigated using a laser Doppler vibrometer (LDV). Significant disk vibration reductions are attained while a shroud is installed onto a disk at certain disk rotation speeds. PESs are also measured for the cases with and without an air shroud during servo implementation. Reductions of PESs are observed when an air shroud is installed at some disk rotation speeds.

1. Introduction

The high capacity of magnetic recording requires continuous increases in track density, and thus decreases in track error. One of the major contributors of track error is non-repeatable run-out (NRRO) generated from disk flutter and spindle vibration [1–9], which are induced by the unsteady air flow inside the disk stack.

In general, there are two types of disk vibration, i.e., the in-plane vibration and out-of-plane vibration. In-plane disk/spindle vibration, known as unbalanced (0, 1) modes or gyro-modes [2], results from coupled vibration of disk vibration modes and rocking motion of the spindle through bearing deformation. To suppress this vibration, hydrodynamic bearings can be used to replace the traditional ball bearings. It has been described by Zang and Hatch [2] that the damping of hydrodynamic bearing is two-order-of-magnitude larger than that of ball bearings. Out-of-plane vibration usually results from disk vibration modes alone. When the

Abbreviations: TMR, track misregistration; PES, position error signal; CFD, computational fluid dynamics; HSA, head suspension assembly; NRRO, non-repeatable run-out; RRO, repeatable run-out

*Corresponding author. Tel.: +65 68748516; fax: +65 67772053.
E-mail address: HE_Zhimin@dsi.a-star.edu.sg (Z. He).

0022-460X/$ - see front matter © 2007 Elsevier Ltd. All rights reserved.
doi:10.1016/j.jsv.2007.09.042

rotational speed exceeds a threshold speed, the air surrounding the spinning disks will excite the disks leading to significant vibration known as disk flutter. The effects of disk flutter on the position error signal (PES) were experimentally shown by McAllister [3]. There are several ways to suppress the flutter or to defer its occurrence, i.e., creating an aerodynamic bearing between the spinning disks and an adjacent stationary surface [10–13], improving the aerodynamic design of base casting [14], increasing the disk stiffness via stacked disks [15], and developing alternative substrate materials [16].

Bittner and Shen [10] proposed an acoustically tuned-mass damper to suppress the disk flutter by use of an air-bearing plate above the top disk, which was set with a large clearance of 635 μm. Ono and Maeda [11] proposed a squeezed air damping by simply setting a flat surface close to the disk with a clearance of less than 300 μm and showed a significant effect of damping the flutter. Deeyiengyang and Ono [12] experimentally investigated the effects of suppressing vibration of a spinning disk/spindle system by applying a squeeze air-bearing film and revealed that the disk flutter vibration can be suppressed further when the air clearance is 120 μm. Du et al. [15] reported an experimental study of disk vibration reduction via stacked disk in magnetic recording system, and achieved a significant improvement in head positioning accuracy. However, the PES reduction in the servo implementation with an air shroud is yet to be reported. The correlations among the shroud design, disk vibration amplitude, functionally air-bearing stiffness, and damping effects have received little attention.

This paper presents an air shroud for suppressing disk vibrations and reducing PES in a magnetic recording system. The shroud partially introduces the air-bearing film to both sides of the disk. Mou et al. [17] already presented computational fluid dynamics (CFD) analysis based on the 3D Navier–Stokes equations and analytical study on the air shroud for disk vibration suppression. This paper reports overall the design, CFD simulation, disk vibration testing, and PES measurement results. These include the velocity and pressure pattern surrounding the disk, the air-bearing stiffness and damping effects with different shroud openings, the power spectrums of the disk vibration at different rotating speeds, and the measured PESs during servo implementation for the cases with and without a shroud. CFD simulation reveals that the air shroud brings functional air-bearing stiffness and damping, which suppress the disk vibrations. Disk vibration and PES measurements show significant reduction of the vibration amplitude and improvement in track misregistration (TMR) while an air shroud is introduced.

For the application of an air shroud in commercial disk drives, Ser and Leong [13] proposed a method and apparatus to control airflow in hard disk drives. This method employs an air separator, which is equivalent to an air shroud, to suppress disk vibration. The difference between the proposed air separator and the air shroud is that there are a number of grooves in the air separator, which can direct the air flow. This paper focuses on investigating the effects of the PES reduction using an air shroud. Therefore the simulation and experiment are based on the designed and prototyped air shroud, which is used for the experimental investigation on a spin stand, rather than a commercial disk drive.

2. Air shroud design and computational fluid dynamics simulation

2.1. The air shroud design and CFD analysis with different openings

A schematic of the shroud design is shown in Fig. 1. When the disk spindle is rotating, an air shroud is installed surrounding the disk to provide an air bearing to the disk. The air bearing would damp the amplitude

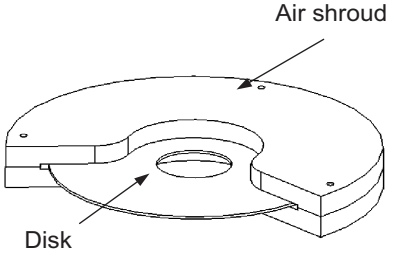

Fig. 1. Schematic of a shroud and a disk.

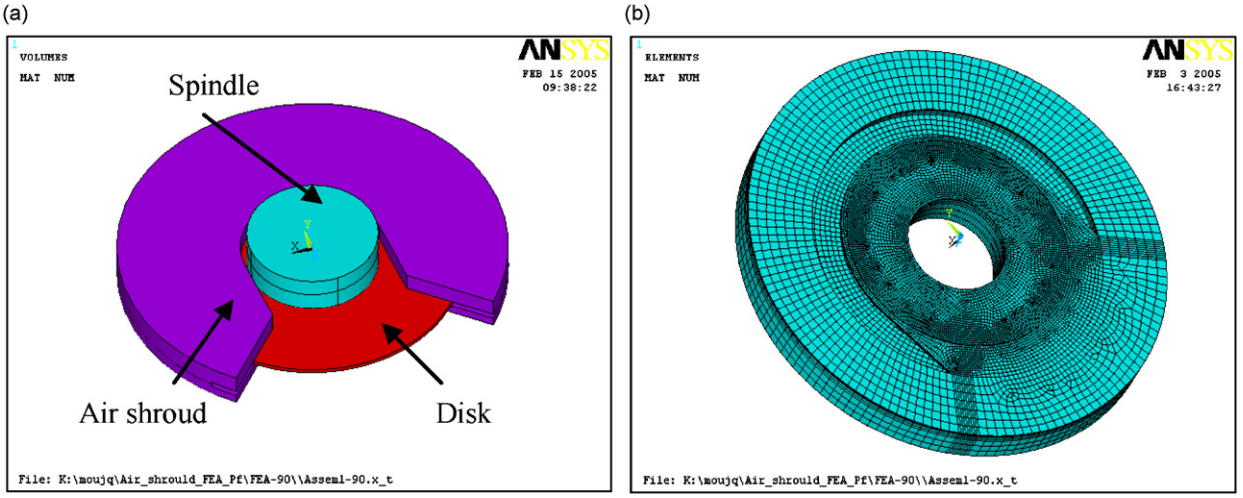

Fig. 2. Air shroud with an opening angle of 90° and the finite element model for CFD analysis. (a) Air shroud with the opening angle 90°, (b) finite element mesh for CFD analysis.

of the disk vibration due to the viscosity of the air. On average, the thickness of the gap between both sides of the disk to the inner shroud surface is 0.60 mm. The open area is used for placing the head actuator assembly.

The air shroud CFD analysis is performed via CFD simulation. The software, ANSYS/Flotran, is employed for the modelling and simulation of a 3.5″ disk rotating at a spin stand. In our study, the 3D-geometry model is composed of the disk, air shroud, and the spindle, as shown in Fig. 2(a). The air flow simulation is performed with the air volume which surrounds the solid volume of disk, shroud, and spindle. To understand the influence of the air shroud opening angles on the air flow velocity pattern and air pressure distribution, CFD simulations are carried out for three shroud opening angles, 180°, 135°, and 90°, separately with a shroud–disk vertical gap of 0.6 mm and a lateral gap of 2 mm at a disk rotational speed of 10,000 rev/min.

The steady-state simulation is performed based on the 3D Navier–Stokes equations with the K-epsilon turbulent model. The FEM model is constructed with hexagonal brick-type element and finer mesh is applied around the disk–shroud area, especially in the narrow gap between the disk–shroud walls. To focus on effects of the air shroud structure and reduce the simulation time, the head suspension assembly (HSA) is not involved in the finite element model. The finite element model for the air shroud with an opening angle of 90° is shown in Fig. 2(b). The rotational velocity of 10,000 rev/min is applied to the nodes at the disk surface with a macro-program written in ANSYS APDL language. The CFD simulation results for the air shroud with different openings are shown in Figs. 3–5. The simulation results demonstrate that the air shroud with the opening angle of 90° has the most uniform air flow pattern and pressure distribution of the three cases.

2.2. *The functional air-bearing stiffness and damping calculation with the CFD analysis*

As the disk rotates with a high rotational speed and the air flow is dominated by the turbulence effects, the traditional calculation method for the air-bearing stiffness and damping based on the simplified Reynolds equation is not adequate for the air shroud [18,19]. To calculate the functional air-bearing stiffness and damping of the shroud, a small disturbance of displacement 10 μm and velocity 1 mm/s in the axial direction of the spindle is applied to the shroud separately in the finite element model for CFD simulation. The variance of the air pressure is obtained after the simulation. The stiffness and damping of the air shroud are then calculated with the change of the integrated force actuated on the disk surface. The stiffness and damping of the air shroud with different opening angles for disk rotational speed 10,000 rev/min are shown in Fig. 6. It is found that with the decreasing of the shroud opening angle from 180° to 90°, the functional air-bearing

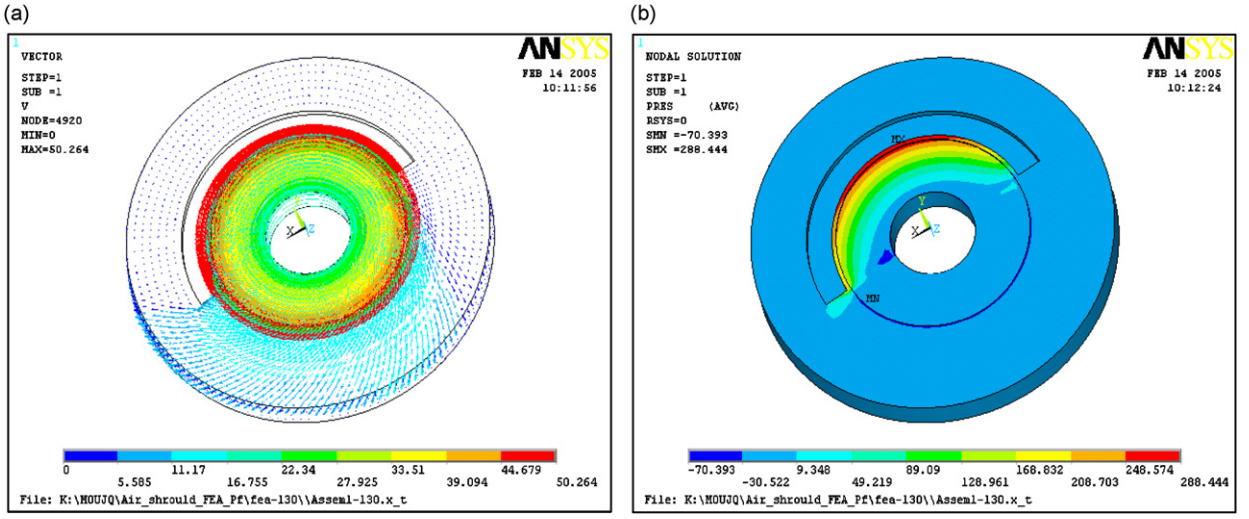

Fig. 3. Air flow velocity and pressure of the air shroud with an opening angle of 180°. (a) Velocity pattern, (b) pressure distribution.

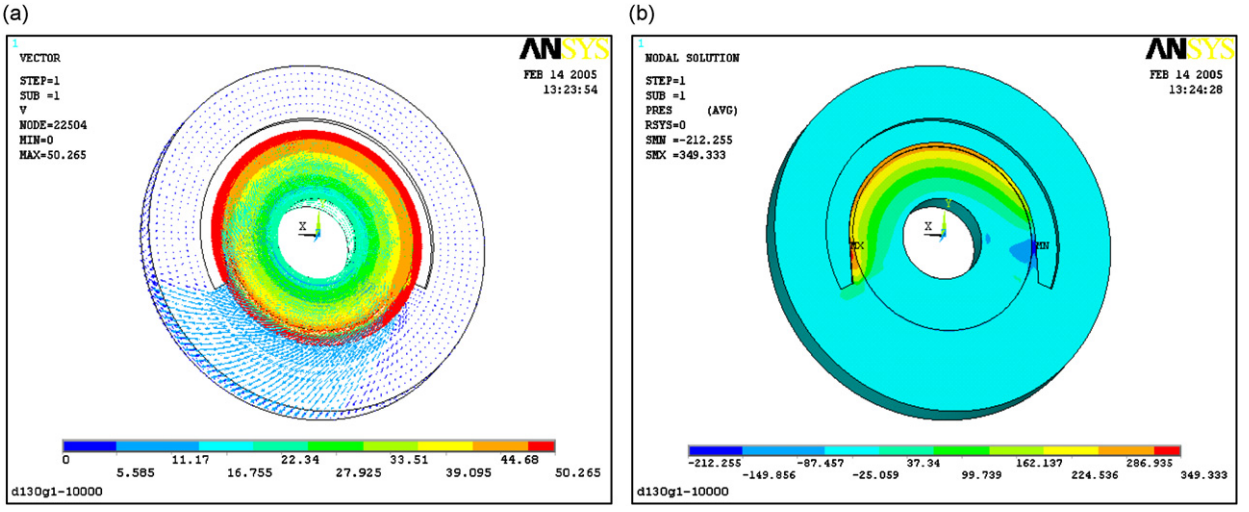

Fig. 4. Air flow velocity and pressure of the air shroud with an opening angle of 135°. (a) Velocity pattern, (b) pressure distribution.

stiffness of the shroud is increased from 0.13 to 0.25 N/mm, and the damping is improved from 0.93 to 1.09 N m/s. The simulation results demonstrate that the air shroud with a smaller opening angle has better bearing stiffness and damping. Therefore, the air shroud opening angle should be minimized under the constraint of the work space of the HSA.

To investigate the correlation between shroud–disk spacing and the functional air-bearing stiffness and damping of the shroud, more CFD simulations are carried out for the air shroud with a 90° opening angle at a disk rotational speed of 10,000 rev/min. The vertical gap between the disk and shroud is gradually changed from 0.25 to 0.85 mm. The influences of the vertical gap between the disk and shroud on the stiffness and damping of the air shroud are shown in Fig. 7, which indicates that the narrower disk–shroud vertical gap leads to greater stiffness and damping of the air shroud. Therefore, the smaller disk–shroud spacing has better effectiveness on the disk vibration suppression, because of greater enhancement of the overall stiffness and damping of the disk spindle system.

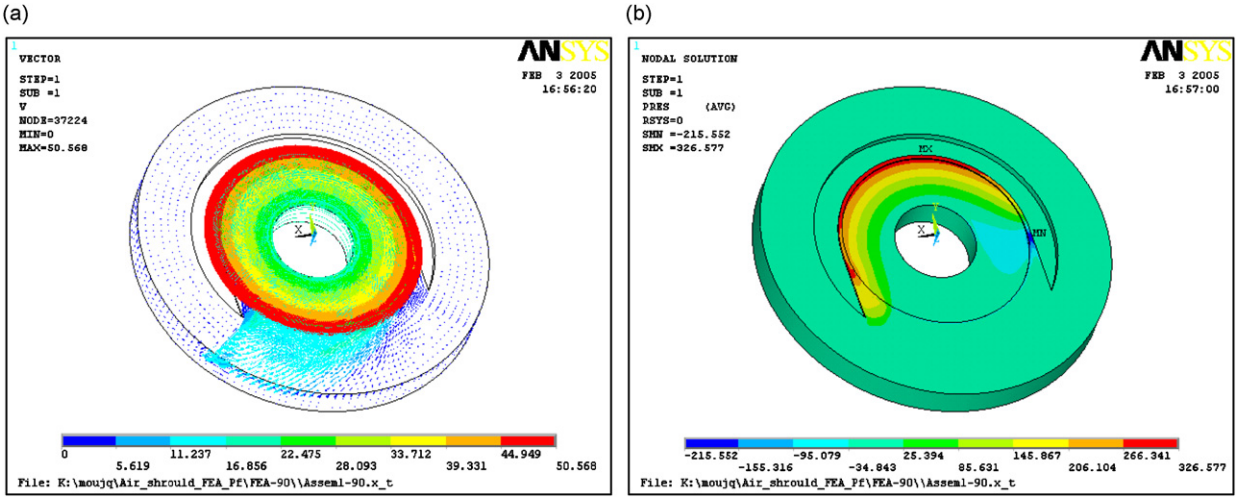

Fig. 5. Air flow velocity and pressure of the air shroud with an opening angle of 90°. (a) Velocity pattern, (b) pressure distribution.

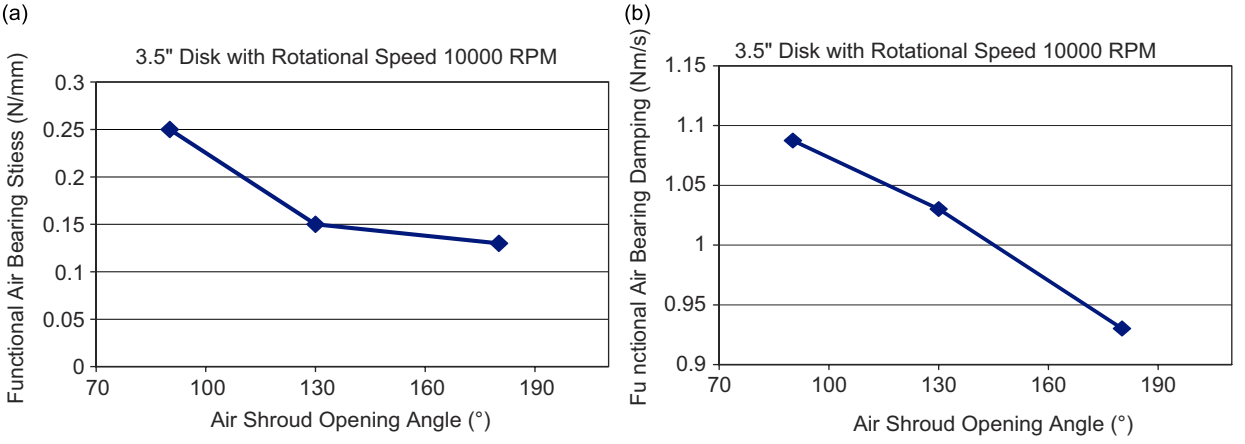

Fig. 6. Stiffness and damping of the air shroud with different opening angles: (a) the functional air-bearing stiffness and (b) the functional air-bearing damping.

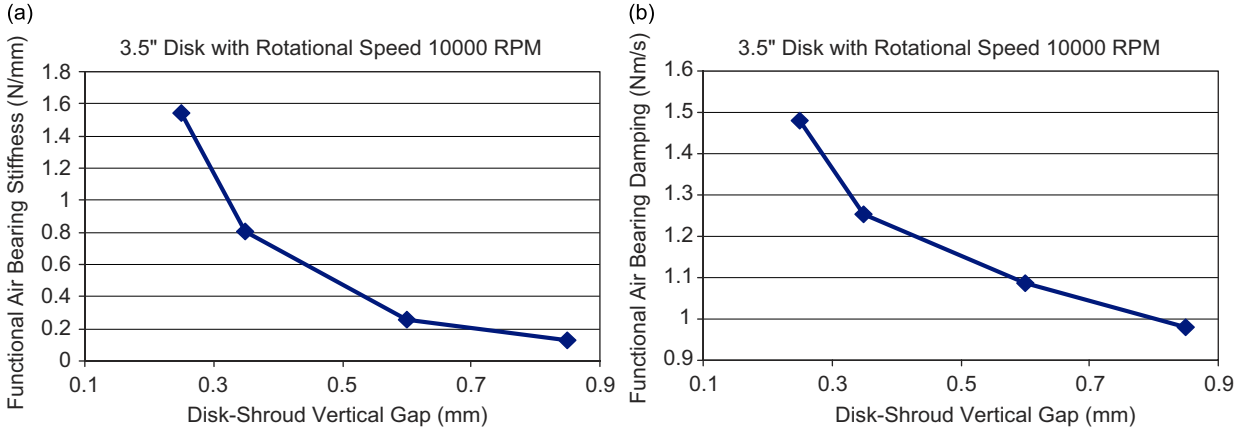

Fig. 7. Stiffness and damping of the air shroud versus shroud–disk vertical gap: (a) the functional air-bearing stiffness and (b) the functional air-bearing damping.

3. Disk vibration measurement

3.1. Experimental setup

Fig. 8 shows the experimental setup of the air shroud assembled to the Guzik spin stand [20]. Laser Doppler vibrometer (LDV) and dynamic signal analyzer (DSA) are used to measure the power spectrum of a point at the edge of the open area of the disk at different rotation speeds. The measured disk is 3.5 in, with glass substrate, thickness 1.27 mm. Before the spectrum measurement, the disk spindle system is balanced.

3.2. Vibration measurement results

Figs. 9–12 show the displacement spectrums of the disk with and without a shroud at 4800, 6000, 8400, and 10,200 rev/min, respectively. The disk vibration modes are denoted as T_i ($i = 1,\ldots, n$). It is obviously the disk vibration reduction for the disk rotation speed at 4800 and 6000 rev/min are significant. All the vibration modes shift slightly lower for the disk spindle assembly with an air shroud. For different vibration modes, the reduction levels are different. The reduction level of the disk vibration also depends on, as reported by Ono and Maeda [11], the gap thickness, radial length and the angular length of air-bearing film. Another observation is that the disk vibration frequencies shift lower by 2–3% when an air shroud is used. This agrees with the testing results reported by Bitter and Shen [10] by using aerodynamic bearings. The shifts are due to the amplified inertia of the air in the air bearing that behaves like an incompressible fluid at the disk mode resonance frequencies. It is also observed that with increasing of the spindle rotation speed, the disk vibration reduction level using the air shroud does not increase accordingly. This is likely due to the air turbulence effect. Generally as the spindle rotation speed increases, more air turbulence is introduced. Experimental study proves that the air velocity surrounding the disk area does not always increase accordingly with the increasing disk rotation speed [21].

4. Measurement of position error signal

The PES is measured with and without the air shroud installed onto the disk spindle assembly, which is mounted on the spindle motor of the Guzik spin stand 1701A. To reflect the effectiveness of the shroud

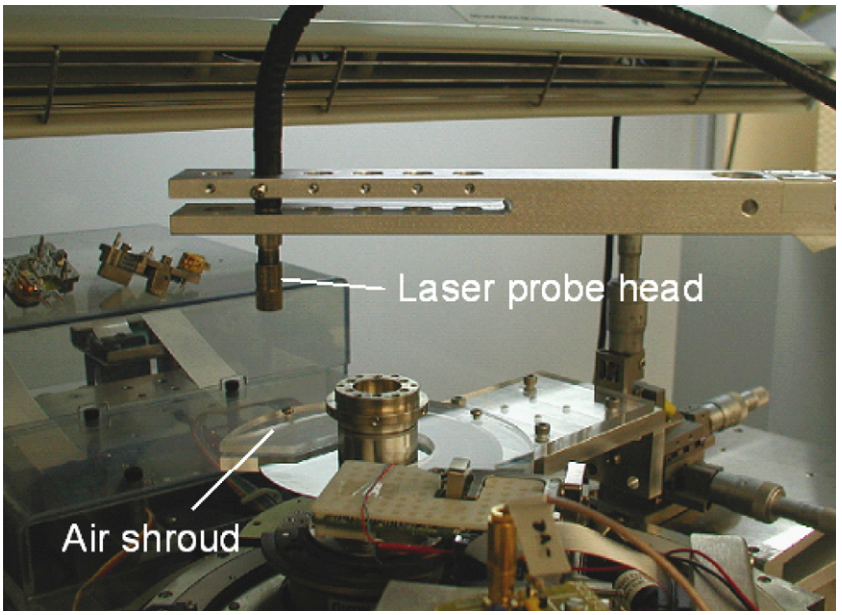

Fig. 8. Experimental setup for spectrum measurement.

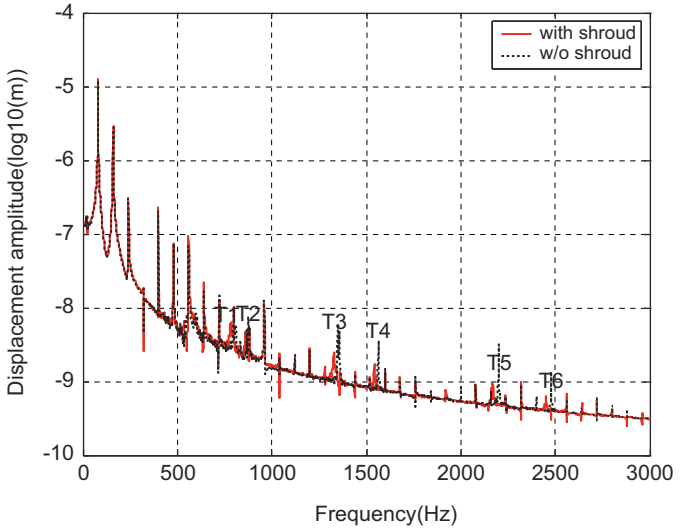

Fig. 9. Displacement spectrum of a 3.5 in thin disk with and without a shroud at 4800 rev/min.

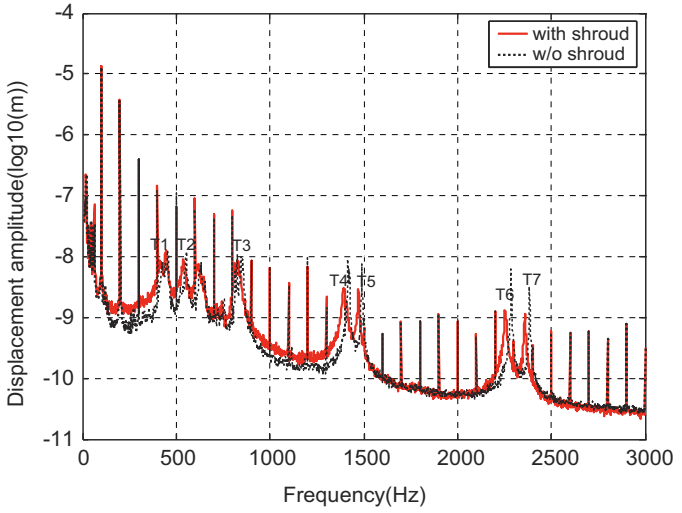

Fig. 10. Displacement spectrum of a 3.5 in thin disk with and without a shroud at 6000 rev/min.

exactly, the PES with and without the air shroud is measured from the same servo information, which is written when the air shroud is removed. The procedure of the measurement is as follows: (1) write the servo information on the disk without the air shroud, (2) read PES and measure it in time domain or frequency domain, (3) insert the air shroud, (4) read PES again and measure it in time domain or frequency domain, (5) change the rotational speed of the motor. Repeat steps 1–4. To calculate the PES, M traces of the PES are collected and denoted by PES_i ($i = 1, \ldots, M$). The repeatable run-out (RRO) and NRRO are then given by

$$\mathrm{RRO} = \frac{1}{M}\sum_{i=1}^{M} \mathrm{PES}_i, \mathrm{NRRO}_i = \mathrm{PES}_i - \mathrm{RRO}. \tag{1}$$

The measurements for the spindle rotational speed at 4800, 6000, 8400, and 10,200 rev/min are presented.

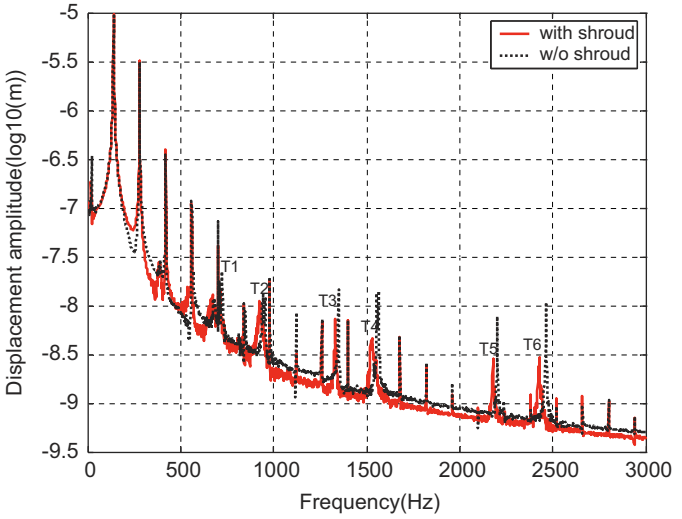

Fig. 11. Displacement spectrum of a 3.5 in thin disk with and without a shroud at 8400 rev/min.

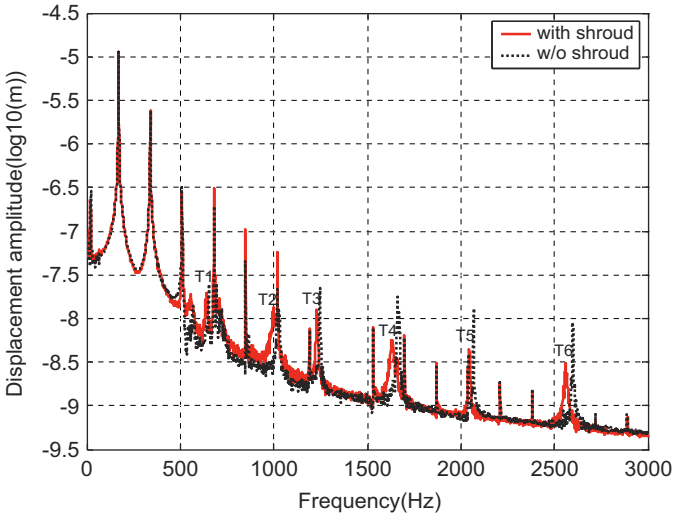

Fig. 12. Displacement spectrum of a 3.5 in thin disk with and without a shroud at 10,200 rev/min.

4.1. Evaluation at 4800 rev/min

Calculated from the collected PES data, the power spectra of the NRRO is plotted in Fig. 13. The disk vibration modes are denoted by T1–T6. We can observe the reduced disk vibration modes T1–T3 and T5. T4 is not clear and thus not marked. It is noted that there is a shift around 1800 Hz in Fig. 13, which randomly occurs and the writing process at a different time may cause such a shifting. The standard deviation (or σ-value) of NRRO is 0.1037 without the air shroud and 0.1015 with the air shroud, about 2.1% improvement achieved. A slight improvement is achieved. In conclusion, the amplitude of some disk vibration modes is indeed reduced via the air shroud, while from the PES there is no remarkable improvement.

4.2. Evaluation at 6000 rev/min

The PES data are collected and the power spectrums of the NRRO with and without the air shroud are shown in Fig. 14. The disk vibrations T3–T5 are clearly reflected in Fig. 14, and the others are not

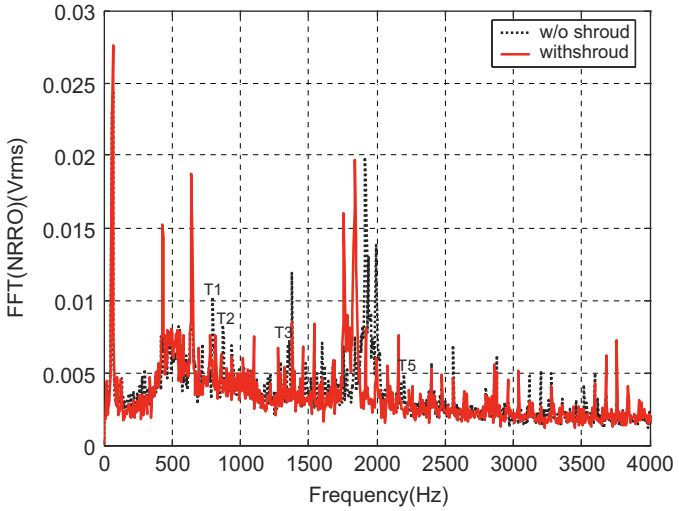

Fig. 13. NRRO power spectrum (4800 rev/min).

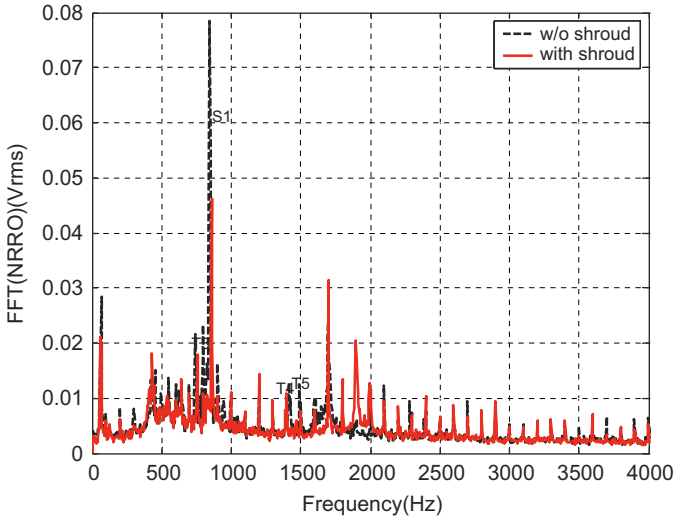

Fig. 14. NRRO power spectrum (6000 rev/min).

obvious. It is observed that one vibration mode, denoted by S1, reduces significantly with the air shroud. This reduction is likely caused by a better interaction of the disk and the slider. The standard deviation of NRRO is 0.1621 without the air shroud and 0.1400 with the air shroud, i.e., improved by 13.6%. Both disk vibration testing and the measured PES show that the air shroud works effectively at 6000 rev/min.

4.3. Evaluation at 8400 rev/min

The power spectrum of the NRRO is plotted in Fig. 15. We can observe that the corresponding disk vibration modes T1–T6 are all lowered by the air shroud. T1 and T4 are reduced more obviously in the NRRO. Notice that S1 is reduced greatly again, which however cannot be traced in the disk vibration in Fig. 11. This further verifies that S1 is caused by the disk–slider interaction. The resultant σ value of NRRO is improved from 0.1629 to 0.1528 and by 6.2%.

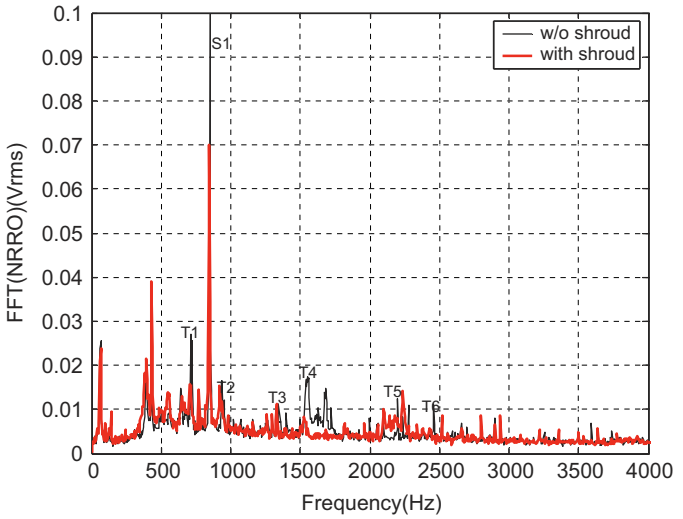

Fig. 15. NRRO power spectrum (8400 rev/min).

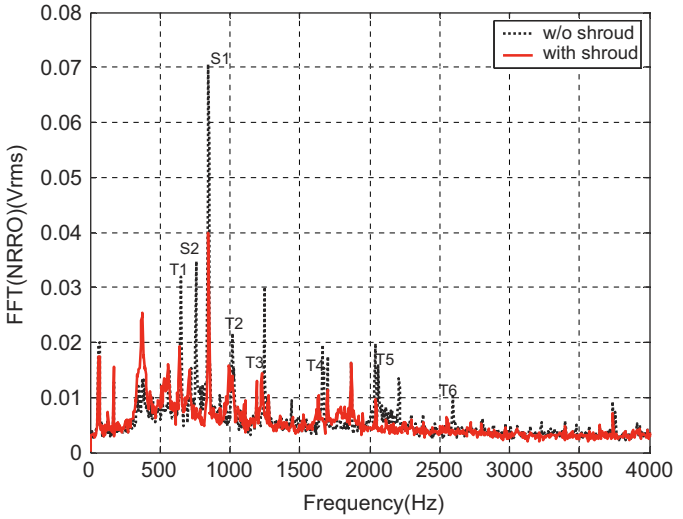

Fig. 16. NRRO power spectrum (10,200 rev/min).

4.4. Evaluation at 10,200 rev/min

Fig. 16 shows the measured PES at a disk rotation speed of 10,200 rev/min. The disk vibration modes T1–T6 are obvious with the amplitude reduced and the frequencies shifted lower when an air shroud is used. Similarly for the slider-related vibration, S1 is reduced significantly. There is another mode S2 in the NRRO spectrum, which is not found in the disk axial vibration in Fig. 12. Thus, S2 is one more slider-related vibration mode and is restrained by the air shroud. As a result, the σ value of the NRRO is reduced from 0.1712 to 0.1543 and a 9.9% improvement is achieved.

The PES reductions for disk spindle assembly with and without an air should at different rotation speeds are listed in Table 1. It can be seen that the effectiveness of the air shroud is different for different rotational speeds. At higher rotational speeds like 8400 or 10,200 rev/min, its effectiveness is smaller than 6000 rev/min. In view of this, mechanical improvement to the air shroud is necessary so that it can work for higher rotational speeds as well. The overall reduction of disk vibration and PES reductions are due to the damping effects.

Table 1
Measured PES, with and without an air shroud at different rotation speeds

Rotation speed (rev/min)	4800	6000	8400	10,200
PES without an air shroud (volt)	0.1037	0.1621	0.1629	0.1712
PES with an air shroud (volt)	0.1015	0.1400	0.1528	0.1543
PES reduction with an air shroud (%)	2.1	13.6	6.2	9.9

5. Conclusions

By CFD simulation, experimental investigation of the disk vibration, measurement of PES and of the disk spindle assembly with and without an air shroud, the following conclusions are supported:

(1) CFD simulation quantifies the pressure and velocity patterns of the disk spindle assembly with an air shroud for different openings. The air shroud with a smaller opening angle and disk–shroud spacing has more uniform air flow pattern and pressure distribution.
(2) An air shroud with a smaller opening and disk–shroud spacing demonstrates better performance in the functional air-bearing stiffness and damping.
(3) An air shroud can reduce the disk vibration while the disk spindle is spinning. The reduction level of disk vibration depends on the design parameters, such as the air gap between the shroud surface and the disk surface. The vibration reduction levels are different for different modes.
(4) The air shroud lowers the resonant frequency of disk vibration about 2–3%. This agrees with previous investigation on disk vibration suppression through aerodynamic bearings. The shift is independent of the spin speed.
(5) With the current shroud design, the measurement on PES power spectrum reveals an air shroud can reduce the PES level. The reduction level relates the disk spindle rotation speed. An improvement of 13.6% of the position accuracy has been achieved at the rotation speed of 6000 rev/min.

References

[1] R. Ehrlich, D. Curran, Major HDD TMR sources and projected scaling with TPI, *IEEE Transactions on Magnetics* 35 (2) (1999) 885–891.
[2] Y. Zang, M.R. Hatch, On the whirl dynamics of hydrodynamic bearing spindle in information storage systems, *Proceedings of the 7th Annual Information Storage and Processing Systems Symposium*, ASME ISPS 2, 1996, pp. 73–84.
[3] J.S. McAllister, The effect of disk flutter resonances on track misregistration in 3.5 inch disk drives, *IEEE Transactions on Magnetics* 32 (3) (1996) 1762–1766.
[4] T. Hasegawa, H. Du, H. Osawa, H. Nishimura, T. Oe, Dynamic analysis of a disk–spindle system in hard disk drive, *IEEE Transactions on Magnetics* 39 (2) (2003) 784–789.
[5] L. Guo, Y.-J.D. Chen, Disk flutter and its impact on HDD servo performance, *IEEE Transactions on Magnetics* 37 (2) (2001) 866–870.
[6] Y.-B. Chang, D.-K. Park, N.-C. Park, Y.-P. Park, Prediction of Track misregistration due to disk flutter in hard disk drives, *IEEE Transactions on Magnetics* 38 (2) (2002) 1441–1446.
[7] J.Y. Shen, C.W. Tseng, I.Y. Shen, Vibration of rotating disk/spindle systems with flexible housing/stator assemblies, *Journal of Sound and Vibration* 271 (3–5) (2004) 725–756.
[8] G. Guo, J. Zhang, Feedforward control for reducing disk-flutter-induced track misregistration, *IEEE Transactions on Magnetics* 39 (4) (2003) 2103–2108.
[9] S. Lim, Finite element analysis of flexural vibrations in hard disk drive spindle systems, *Journal of Sound and Vibration* 233 (4) (2000) 601–616.
[10] H. Bittner, I.Y. Shen, Taming disk/spindle vibration through aerodynamic bearings and acoustically turned-mass dampers, *IEEE Transactions on Magnetics* 35 (2) (1999) 827–832.
[11] K. Ono, E. Maeda, Suppression of disk flutter by a squeeze air-bearing plate, *Journal of Information and Process Systems* 2 (1/2) (2000) 33–40.
[12] S. Deeyiengyang, K. Ono, Suppression of resonance amplitude of disk vibration by squeeze air bearing plate, *IEEE Transactions on Magnetics* 37 (2) (2001) 820–825.
[13] S.C. Ser, W.H. Leong, Method and apparatus to control airflow in hard disk drives, US Patent Application, US 2006/0114603 A1 (2006).

[14] B. Heo, I.Y. Shen, J. Riley, Reducing disk flutter by improving aerodynamic design of base casting, *IEEE Transactions on Magnetics* 36 (5) (2000) 2222–2224.
[15] C. Du, W.E. Wong, G.X. Guo, Experimental study of disk vibration reduction via stacked disks, *Journal of Sound and Vibration* 301 (1–2) (2007) 226–235.
[16] A. Daugela, K. Tonder, F.E. Talke, Flutter evaluation of aluminum boron carbide and aluminum disks, *Journal of Information and Process Systems* 1 (4) (1999) 299–302.
[17] J.Q. Mou, L.C. Lee, G.X. Guo, Evaluation of an air shroud for rotating disk vibration suppression, *Proceedings of the 7th International Power Engineering Conference*, Singapore, Vol. 2, 2005, pp. 1153–1158.
[18] B.J. Hamrock, *Fundamentals of Fluid File Lubrication*, McGraw-Hill Inc., 1994.
[19] M. Tatewaki, N. Tsuda, T. Maruyama, An analysis of disk flutter in hard disk drives in aerodynamic simulations, *IEEE Transactions of Magnetics* 37 (2) (2001) 842–846.
[20] Guzik Company Website [online], Spin Stand Products Information, 〈http://www.guzik.com/〉.
[21] T.H. Yip, C.K. Tan, Y.K. Kuan, Behavior of spiral flow structures along the trailing edges of E-block arms under increasing airflow, *IEEE Transactions on Magnetics* 42 (10) (2006) 2591–2593.